Multi-compartment model of synaptic plasticity

E. Paxon Frady

We introduce a biophysical model of a neuronal network that can accurately replicate many classical plasticity experiments. The model uses Hodgkin and Huxley dynamics across multiple compartments and uses a simple learning rule based on calcium signaling. We report replications of many of the results from Markram et al, 1997, Bi & Poo, 1998, Sjostrom et al, 2001, and Golding et al, 2002, which cover a vast set of plasticity induction protocols and mechanisms.

Introduction

The modification of synaptic connections is thought to underlie the process of learning in the brain. Recently, many of the details of this process have been discovered and a large range of governing principles have been found that regulate long-term potentiation and depression. A major breakthrough of this process has been the discovery that the timing between pre and post synaptic action potentials has an effect on the conductance properties of synapses (1; 2; 3). Spike-timing dependent plasticity (STDP) has been a major area of theoretical study in recent years, but although a good step, STDP is only a small part of the regulatory mechanisms that generate synaptic plasticity.

In this paper we introduce a very detailed biophysical description of a neuron and network. We show that this model can reproduce a large variety of experimental results of synaptic plasticity in great detail. We would like to suggest a model such as this as a starting point for a complete description of neural activity, and as a point from which to study the mechanisms of plasticity and neuronal coding. From a very detailed and accurate description of neural behavior it will be easier for theorists to pull out abstractions of the model and understand the actual underlying functions neurons compute.

Methods

Multiple Compartments

For a more complete description of a neuron, the model uses multiple compartments to describe the state variables of a neuron. Axonal compartment and dendritic compartments have different properties determined by the density of channels. Each dendritic compartment will have one parent, which will either be an axonal compartment or a descendant of an axonal compartment. Each compartment can have several children. The voltage interactions across compartments are determined by passive conductance of ions:

$$\frac{dV}{dt} = \lambda\left(\left(V_{parent} - V\right) + \sum\left(V_{child} - V\right)\right)$$

where λ is a compartmentally determined length constant.

Calcium flux across compartments is similarly determined, but instead of linear voltage-dependent conductance properties the driving force acting on calcium ions is dependent on both voltage and calcium concentration as determined by the Goldman-Hodgkin-Katz equation:

$$\frac{d[Ca^{2+}]}{dt} = \lambda_{Ca}\left(-GHK(V - V_{parent}, [Ca^{2+}], [Ca^{2+}_{parent}]) - \sum GHK(V - V_{child}, [Ca^{2+}], [Ca^{2+}_{child}])\right)$$

where λ_{Ca} is a compartmentally determined length constant. GHK is the Goldman-Hodgkin-Katz function which describes the driving force of a charged ion as determined by both voltage and concentration:

$$GHK(\Delta V, [Ca^{2+}]_i, [Ca^{2+}]_o) = \frac{2F\Delta V}{RT}\frac{\left([Ca^{2+}]_i - [Ca^{2+}]_o \exp\left(-\frac{2F\Delta V}{RT}\right)\right)}{1 - \exp\left(-\frac{2F\Delta V}{RT}\right)}$$

where F is Faraday's constant, R is the gas constant, T = 298 K is the temperature in Kelvin. ΔV describes the difference in voltage across the two locations, and $[Ca^{2+}]_I$, $[Ca^{2+}]_o$, are the concentrations of Calcium in the two locations.

Voltage Dynamics

The voltage dynamics of each compartment is determined by the concentration and kinetics of several conducting channels. It is governed by the kinetics equation:

$$C_M \frac{dV}{dt} = \bar{g}_{Na} m^3 h\,(E_{Na} - V) + \bar{g}_K n^4 (E_K - V) + g_L(E_L - V) + I_{NMDA} + I_{AMPA} + I_{VGCC} + I_{ext}$$

where C_M is the membrane capacitance. The first three terms are the familiar Hodgkin and Huxley equations describing action potentials (4). The current I_{ext} is the external input current used to drive the voltage for experimental purposes.

Current determined by the NMDA receptor is described as follows (5):

$$I_{NMDA} = g_{NMDA-V}\, r_{NMDA} B(V)(E_{NMDA} - V)$$

where $g_{NDMA\text{-}V}$ is the maximal conductance associated with the channel (channel density). E_{NMDA} describes the reversal potential of the NMDA channel and r_{NMDA} describes the open fraction of the population of NMDA channels, which is dependent on the amount of neurotransmitter released from the presynaptic neuron. The kinetics of r_{NMDA} are:

$$\frac{dr_{NMDA}}{dt} = \alpha_{NMDA} T(V_{pre})(1 - r_{NDMA}) - \beta_{NMDA} r_{NMDA}$$

where α_{NMDA} , and β_{NMDA} are the rate constants of the channel, and $T(V_{pre})$ is the amount of neurotransmitter released from the presynaptic terminal:

$$T(V_{pre}) = \frac{T_{max}}{1 + \exp\left(-\frac{V_{pre} - V_p}{K_p}\right)}$$

where T_{max} is the maximum amount of transmitter that can be in the synaptic cleft, V_{pre} is the pre-synaptic voltage, K_p describes the steepness and V_p sets the value at which the function is half activated.

The NMDA channel is also subject to a blockage of extracellular magnesium. This blockage is described by B(V) and is a function of the post-synaptic voltage:

$$B(V) = \frac{1}{1 + 0.288 \exp(-0.062V)\,[Mg^{2+}]_o}$$

where $[Mg^{2+}]_o$ is the concentration of extracellular magnesium.

The AMPA channel is described in a similar manner, but is not subject to blockage by extracellular magnesium (5):

$$I_{AMPA} = g_{AMPA-V} r_{AMPA} (E_{AMPA} - V)$$

where $g_{AMPA\text{-}V}$ is the maximum conductance of the AMPA channels. This value is modified by LTP and LTD which will be described later. E_{AMPA} describes the reversal potential of the AMPA channel. Similar to the NMDA channel the open fraction, r_{NMDA}, kinetics are described by:

$$\frac{dr_{AMPA}}{dt} = \alpha_{AMPA} T(V_{pre})(1 - r_{AMPA}) - \beta_{AMPA} r_{AMPA}$$

where α_{AMPA}, β_{AMPA} are the rate constants of the channel and $T(V_{pre})$ is the amount of neurotransmitter released from the presynaptic cell as described earlier.

Finally, the current through the voltage-gated calcium channels (I_{VGCC}) takes the form (6):

$$I_{VGCC} = g_{VGCC-V} GHK(V, [Ca^{2+}]_{in}, [Ca^{2+}]_{out}) m_{VGCC}^2 h_{VGCC}$$

where g_{VGCC} is a conductance, and the GHK function described earlier is the driving force of the ions through the channel. m_{VGCC} is an activation function, and h_{VGCC} is an inactivation function described by the following kinetics equations:

$$\frac{dX}{dt} = \alpha_X(V)(1 - X) - \beta_X(V) X$$

where α_X, and β_X are the rate constants.

Calcium Dynamics

The calcium dynamics of the model is further separated into synaptic and compartmental calcium. The interaction between the calcium levels in the synapse and the compartment is determined by differences in calcium concentration of the synapse and compartment. To simplify the computation, for each time step the equilibrium concentration of calcium levels is determined and each synapse and the compartment are adjusted towards that equilibrium:

$$Ca_{eq}^{2+} = Ca_{comp} + \sum_{syn} \gamma(Ca_{syn} - Ca_{comp})$$

where Ca_{comp} is the compartmental Calcium concentration, Ca_{syn} is the synaptic Calcium concentration and γ is the ratio of the synaptic volume to the dendritic volume. The calcium levels are then adjusted towards this equilibrium point:

$$\frac{dCa^{2+}}{dt} = \frac{1}{\tau}\left(Ca_{eq}^{2+} - Ca^{2+}\right)$$

where τ is the time constant of the calcium flux.

The calcium concentrations of the compartments and synapses are further governed by the channels in the cell. For the compartments, Calcium concentration is influenced by calcium flux through voltage gated calcium channels, as well as calcium being pumped out of the cell:

$$\frac{d[Ca^{2+}]_{comp}}{dt} = \frac{1}{\tau_{Ca}}\left([Ca^{2+}]_0 - [Ca^{2+}]_{comp}\right) + \Phi_{VGCC}$$

where τ_{Ca} is the decay rate of the calcium concentration towards the equilibrium concentration $[Ca^{2+}]_0$. Φ_{VGCC} describes the calcium concentration flux coming through the voltage gated calcium channel:

$$\Phi_{VGCC} = g_{VGCC-Ca}\, GHK(V_{out} - V, [Ca^{2+}]_{comp}, \left[Ca^{2+}\right]_{out}) m_{VGCC}^2 h_{VGCC}$$

where this equation is identical to the corresponding effect of the VGCC on voltage other than a different constant $g_{VGCC\text{-}Ca}$ which translates the driving force into calcium flux.

The calcium flux in each synapse is determined by calcium that flows through the NMDA and AMPA channels. Calcium leakage in the synapses is ignored, as the connectivity to the compartments and leakage term in the compartments is sufficient to describe this term:

$$\frac{d[Ca^{2+}]_{syn}}{dt} = \Phi_{NMDA} + \Phi_{AMPA}$$

These channels are governed by the same kinetics as in the voltage equations. However, calcium flux differs through the GHK equation describing the driving force, and a different conductance constant:

$$\Phi_{NMDA} = g_{NMDA-Ca} r_{NMDA} B(V) GHK(V_{out} - V, [Ca^{2+}]_{syn}, [Ca^{2+}]_{out})$$

$$\Phi_{AMPA} = g_{AMPA-Ca} r_{AMPA} GHK(V_{out} - V, [Ca^{2+}]_{syn}, [Ca^{2+}]_{out})$$

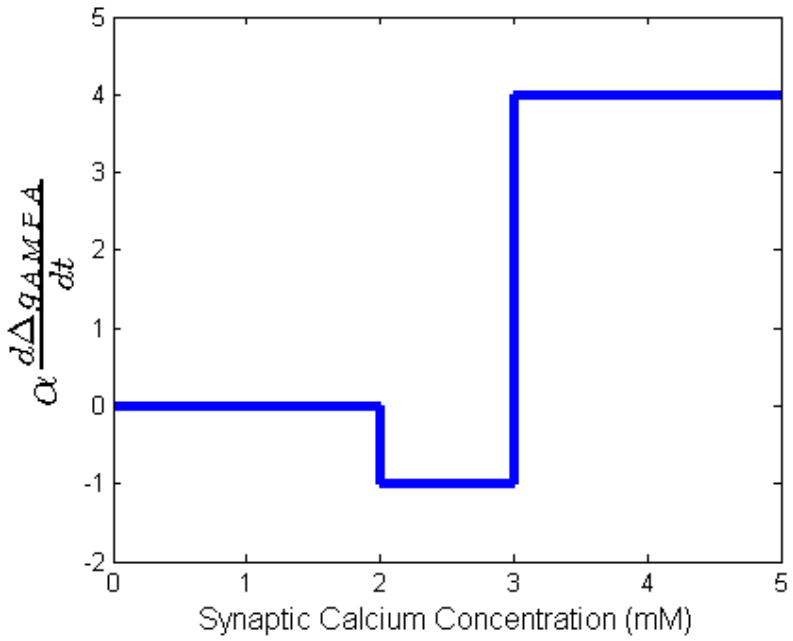

Figure 1 – The Calcium control hypothesis states that the intracellular Calcium concentration determines the change in AMPA receptor conductance for the cell. This is an example of the Ω function used to describe the calcium control hypothesis. In this example Calcium levels between 2-3 mM will lead to depression, but levels above 3 mM will lead to potentiation. Below 2 mM Calcium concentration has no effect on AMPA conductances. (This is just an example and does not reflect actual numbers used in the model).

In these equations, the opening fraction terms, r, as well as the blockage term, B(V), are exactly the same as in the voltage equations. $g_{AMPA\text{-}Ca}$ and $g_{NMDA\text{-}Ca}$ are conductance terms for calcium concentration.

Synaptic Plasticity

Plasticity in each synapse is determined by the Calcium levels in each synapse. Synaptic connections are modified by increasing or decreasing the amount of AMPA receptors in the synapse. This is done by changing the maximum conductance, $g_{AMPA\text{-}V}$, in the I_{AMPA} equation. The translation of Calcium concentration to changes in synaptic conductance is governed by the Calcium control hypothesis (7), which states that low levels of calcium induce LTD and high levels induce LTP. This model uses a direct calculation of the translation from Calcium concentration to AMPA change in ampa conductance based on the sum of two step functions:

$$\frac{d\Delta g_{AMPA}}{dt} = \eta\Omega\left([Ca^{2+}]_{syn}\right) - \frac{1}{\tau}\Delta g_{AMPA}$$

where η is the learning rate, Ω is the calcium control function – an example of which is shown in Figure 1, and τ is the decay rate of the change in conductance. During each timestep the AMPA conductance is changed by the amount Δg_{AMPA}.

Experimental Model

To emulate many properties discovered through experiments in biological systems, a simple two-neuron network was built using the model described above. Each neuron had an axonal compartment and 3

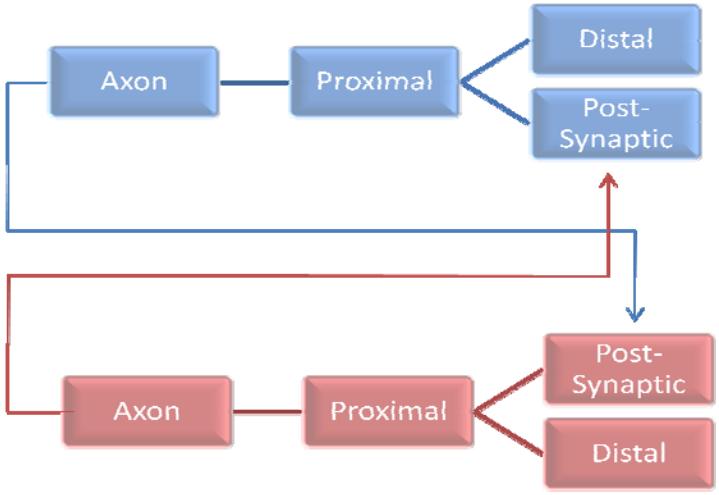

Figure 2 – Connectivity description of the 2 experimental neurons. Each neuron has 4 compartments – 1 axonal and 3 dendritic. The axons are synaptically connected to one of the distal dendritic compartments of the other neuron.

dendritic compartments. The neurons were bidirectionally connected by creating synapses between each axonal compartment and a dendritic compartment on the other neuron. Figure 2 shows the connectivity of the experimental model. Axonal and dendritic compartments contained the same density of voltage-gated calcium channels, but the axonal compartments contained ten times the density of sodium and potassium channels than the dendrites (Full parameter listing described in the appendix).

The model was tested using a similar timing-based pairing protocols as described in many synaptic plasticity experiments (1; 2; 8; 9). The coupled neurons were injected with current pulses lasting 5 ms in the axonal compartments – which were strong enough to elicit action potentials. The time between stimulation of the pairings varied from 0 to 50 ms difference. The parings would be done 5 times at different frequencies – this varied between 2 Hz and 40 Hz. These two parameters were manipulated to resemble parameters used in experiments in real neurons and replicate the results of these experiments with the model.

Results

Spike-Timing Dependent Plasticity

The first experiment sought to replicate the results of Markram et al, 1997. The Markram experiments induced plasticity in two bidirectionally coupled neurons by evoking action potentials in one 10 ms before evoking them in the other. Since they were bidirectionally coupled, this lead to one neuron firing 10 ms before its post-synaptic neuron, and to another neuron firing 10 ms after its post-synaptic neuron. Markram demonstrated that the pre-before-post synapse would potentiate after the pairing protocol, and that the post-before-pre synapse depressed. This same experiment was carried out on the model network and generated potentiation in the pre-before-post synapse, and depression in the post-before-pre synapse. The model used a separation of 10 ms and a pairing frequency of 10 Hz 5 times. The

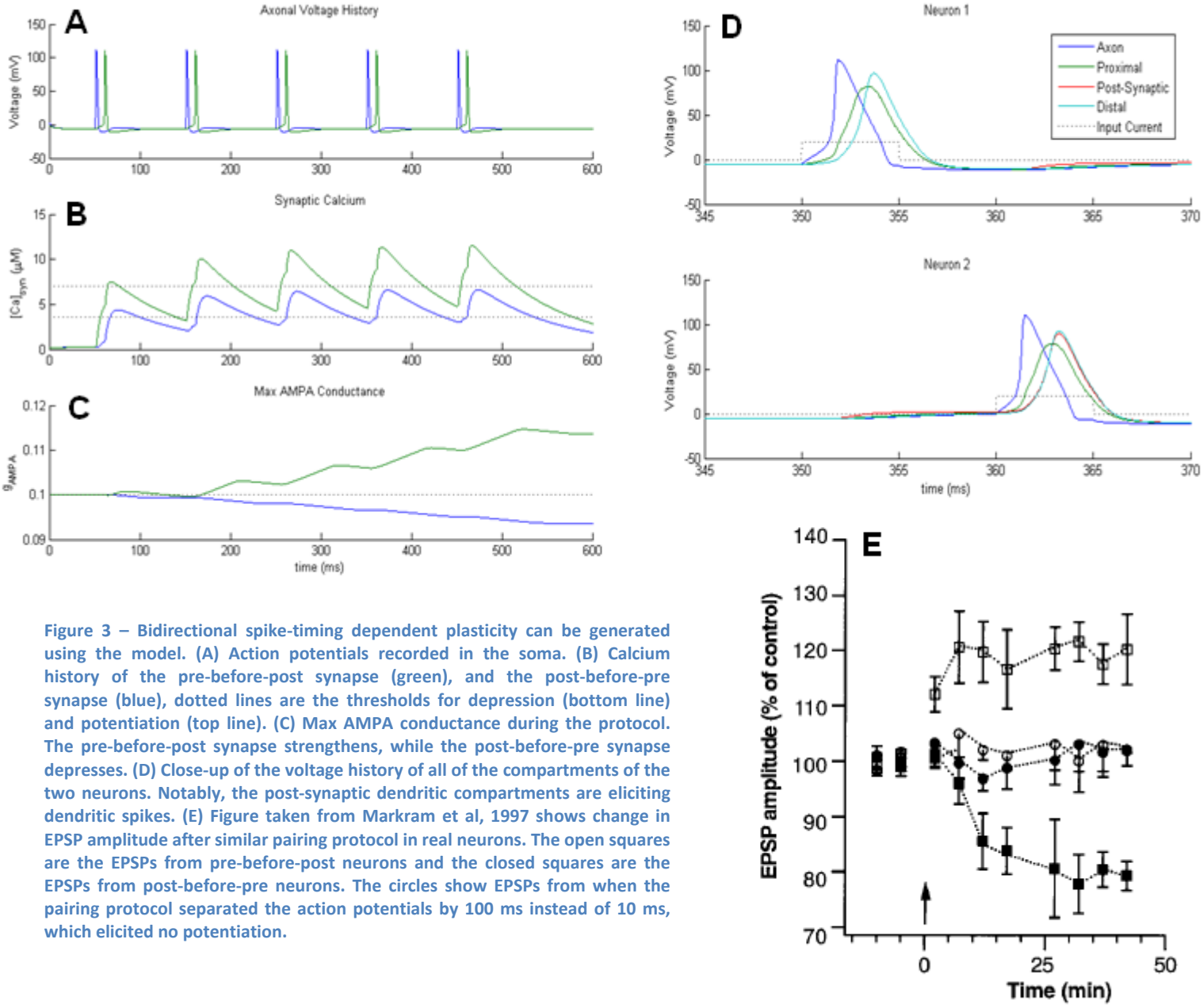

Figure 3 – Bidirectional spike-timing dependent plasticity can be generated using the model. (A) Action potentials recorded in the soma. (B) Calcium history of the pre-before-post synapse (green), and the post-before-pre synapse (blue), dotted lines are the thresholds for depression (bottom line) and potentiation (top line). (C) Max AMPA conductance during the protocol. The pre-before-post synapse strengthens, while the post-before-pre synapse depresses. (D) Close-up of the voltage history of all of the compartments of the two neurons. Notably, the post-synaptic dendritic compartments are eliciting dendritic spikes. (E) Figure taken from Markram et al, 1997 shows change in EPSP amplitude after similar pairing protocol in real neurons. The open squares are the EPSPs from pre-before-post neurons and the closed squares are the EPSPs from post-before-pre neurons. The circles show EPSPs from when the pairing protocol separated the action potentials by 100 ms instead of 10 ms, which elicited no potentiation.

Markram experiment repeated this protocol 10 times every 4 seconds, but the model experiments were only done once. Figure 3 shows the pairing protocol and plasticity results for the model.

The full range of timing-dependence was described by Bi and Poo, 1998. They varied the timing difference between the spikes of neurons and showed how plasticity changed based on the separation of action potentials. Similar work was done later by Sjostrom et al, 2001. Using the same protocol as described in figure 3, the full spike timing curve was generated for the model. Figure 4 shows the complete curve (a 50 ms difference in timing was the maximum amount as the pairings were done at 10 Hz). Similar results were obtained using the model as those demonstrated by the experiments of Bi and Sjostrom. Notably the model showed potentiation between -2 ms and 20 ms timing difference between pre and post-synaptic activity. Outside of this window, however, the model demonstrated depression. The exact timings shown in these curves are determined using various different metrics (by stimulation

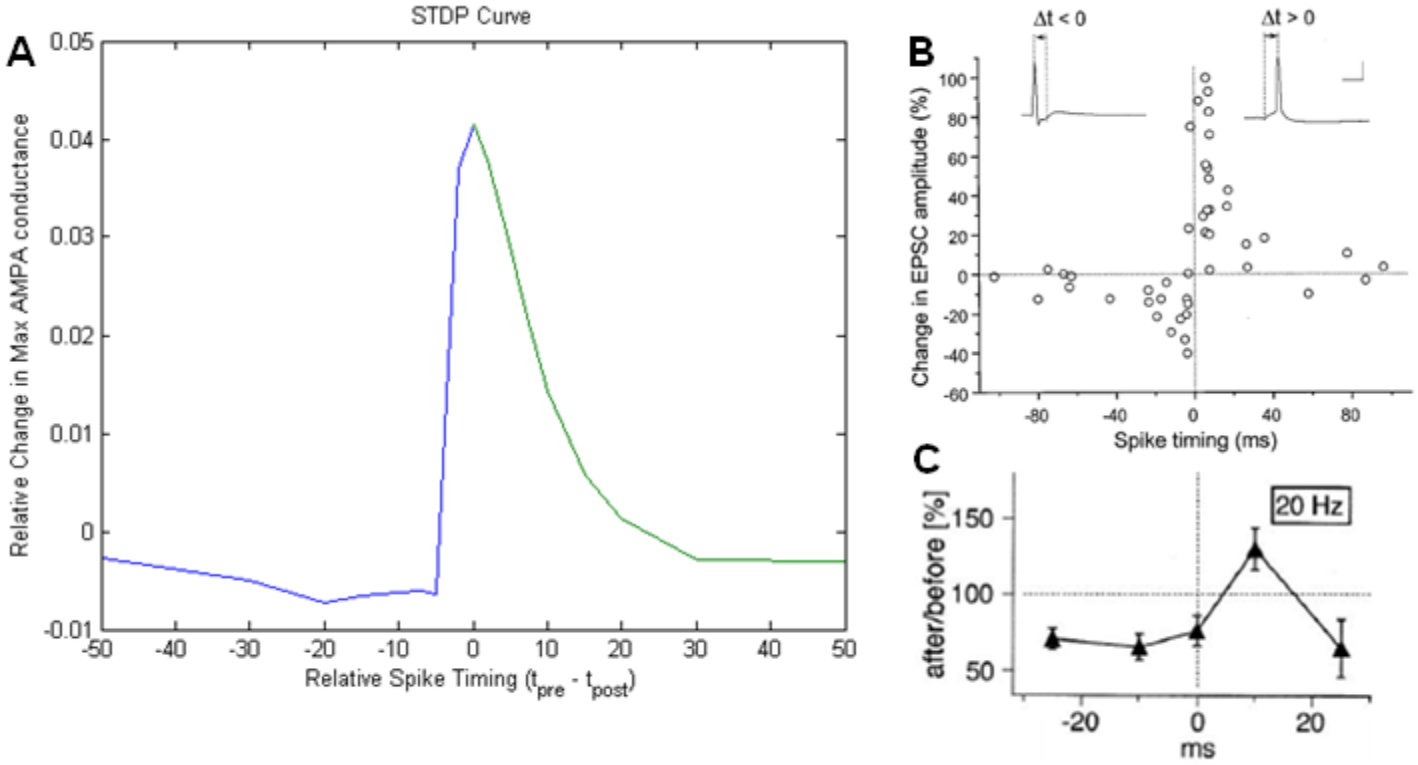

Figure 4 – Spike-timing dependent plasticity curve from model shows similar features as experimental data. (A) STDP curve generated using a similar protocol as described in the Markram experiments, except the timing between stimulations was varied between 0 and 50 ms. The green curve shows the effects of plasticity on the neuron which was stimulated last in the pairing, and the blue curve shows the effects of plasticity on the neuron which was stimulated first in the pairing. The window between -2 ms and 20 ms shows potentiation in the model, while outside of this window shows depression. (B) Data from Bi and Poo, 1998 describing the timing-dependence of LTP and LTD. (C) Data from Sjostrom et al, 2001 which also shows STDP. The data from Sjostrom shows depression outside of the potentiation window, which is similar to the depression observed with the model.

pulse onset, by onset of EPSP, etc) so it is not fair to compare based on this value. Different metrics for timing, or slightly different parameters for the model could be used to explain slight discrepancies observed between the experimental data and the model's data.

Frequency Dependence

Both experiments done by Markram and Sjostrom describe a frequency dependence of plasticity during their induction protocols. This data can also be replicated by the model by varying the stimulation frequency of the pairs of action potentials. The experiments done by Markram shows that increasing frequency demonstrates a threshold like behavior for LTP. Around 10 Hz the amount of plasticity sharply increases from almost 0 and then quickly saturates (Figure 5b). The model demonstrates similar results where the amount of plasticity quickly rises above 5 Hz and reaches a maximum around 15 Hz and then slightly decreases as the frequency increases (Figure 5a). The peak observed in the model is an interesting phenomenon as it suggests that certain sets of parameters give rise to different levels of plasticity sensitivity.

Sjostrom further notices that LTD is abolished at frequencies above 40 Hz. They demonstrate that even with post-before-pre synapses LTP can be induced if the stimulation frequency is high. This data was replicated by the model using the bidirectionally coupled neurons. At high pairing frequency, both synapses potentiated showing the abolishment of LTD at high pairing frequencies (Figure 6c). The data

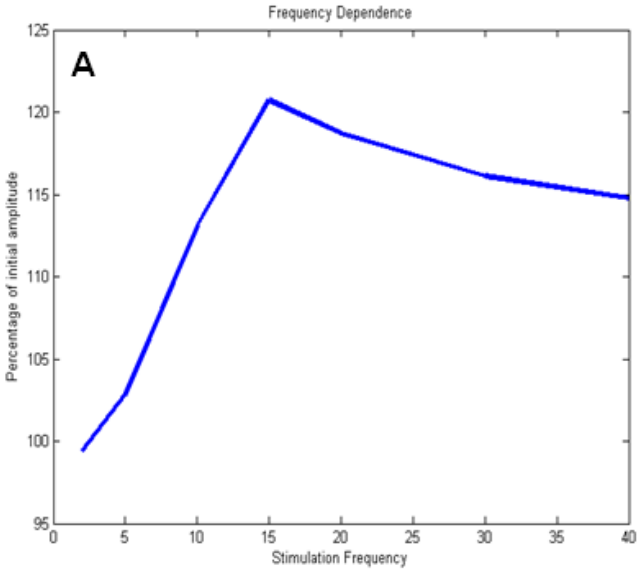

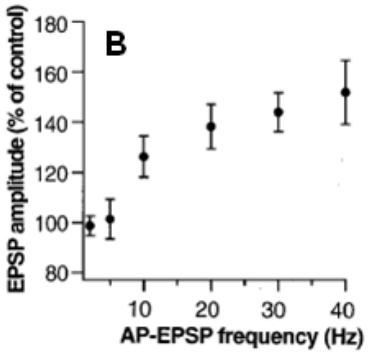

Figure 5 – Frequency dependence. (A) Model data showing the frequency dependence of LTP during the induction protocol. The potentiation amount quickly rise to a max then slowly decreases. (B) Data taken from Markram et al, 1997 showing a sharp onset in potentiation above 10 Hz.

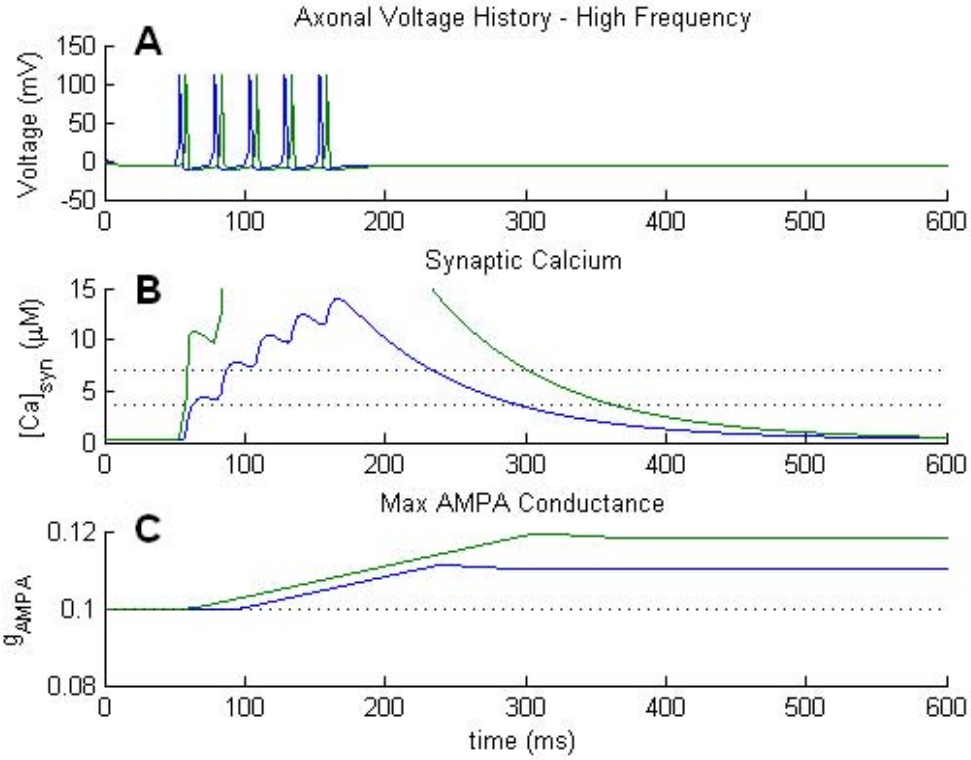

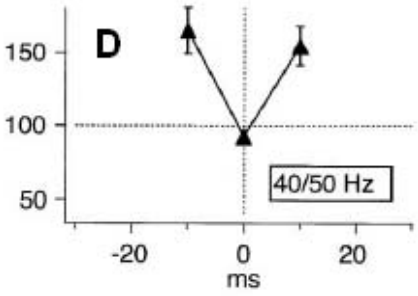

Figure 6 – Abolishment of LTD at high frequencies. (A) Action potentials recorded at soma of model – stimulation frequency is 40 Hz. (B) Calcium history of the pre-before-post synapse (green) and the post-before-pre synapse(blue). (C) Max AMPA conductance during the protocol. Both synapses potentiate at high frequencies. (D) Data taken from Sjostrom et al. 2001 showing that LTD is abolished at stimulation pairings of 40 and 50 Hz.

from Sjostrom also shows that at high frequency no potentiation was observed if the spike timing difference was near 0 ms (Figure 6d). The model was unable to account for this affect as it still lead to potentiation at high frequencies when the timings of the action potentials were brought closer together.

Requirement of Dendritic Spikes

Golding et al 2002, show that dendritic regenerative events – called dendritic spikes, is necessary for LTP in distal dendrites of hippocampal cells. They give strong evidence that LTP is primarily induced during these events by showing that blocking the back-propagating action potential (bAP) can still result in LTP

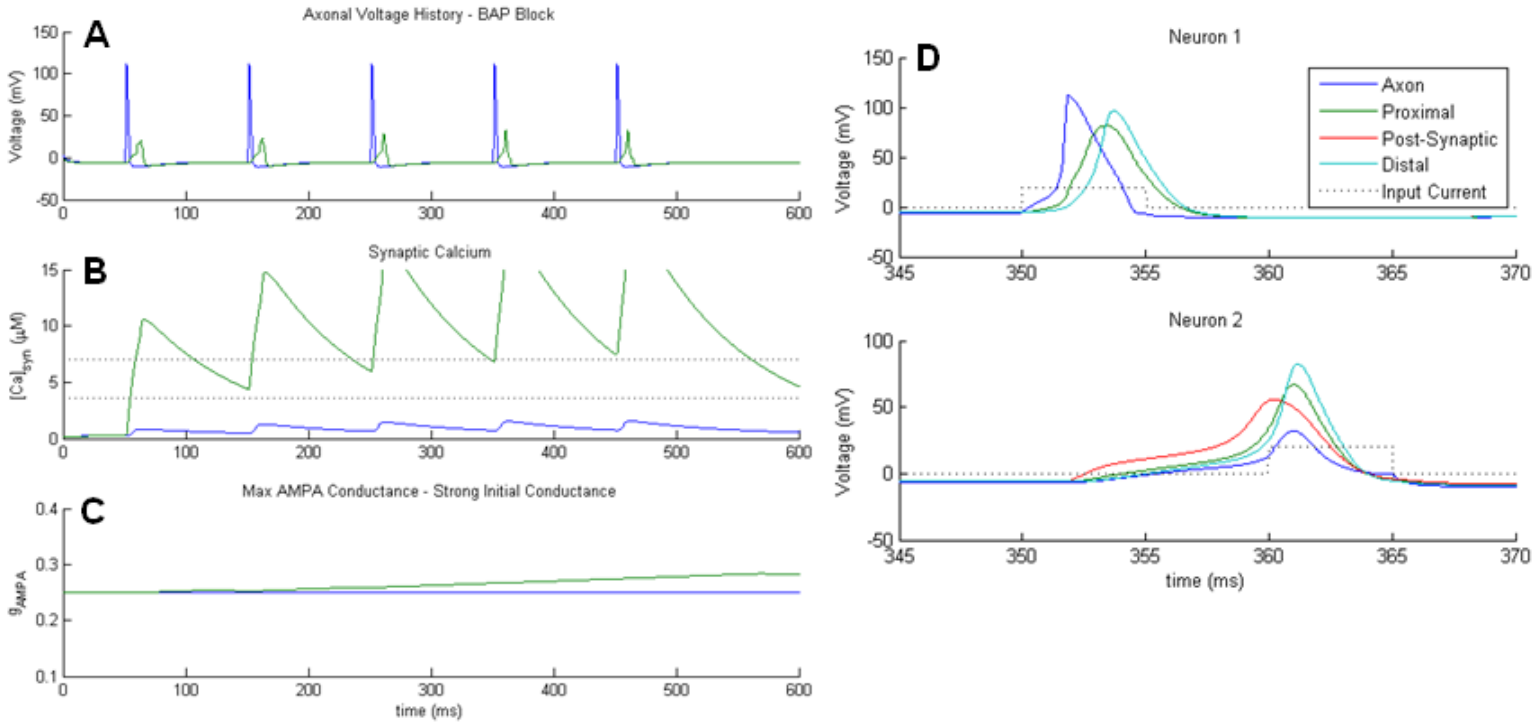

Figure 7 – Strong synapses induce LTP in the absence of bAPs. (A) Voltage history in the somatic compartments of the two neurons. (B) Calcium history of the pre-before-post synapse (green) and the post-before-pre synapse (blue). (C) Max AMPA conductance history of the two synapses. The pre-before-post synapse increases in strength even without the bAP. (D) Close-up of voltage traces for each compartment. The regenerative event of the red trace in Neuron 2 shows the dendritic spike.

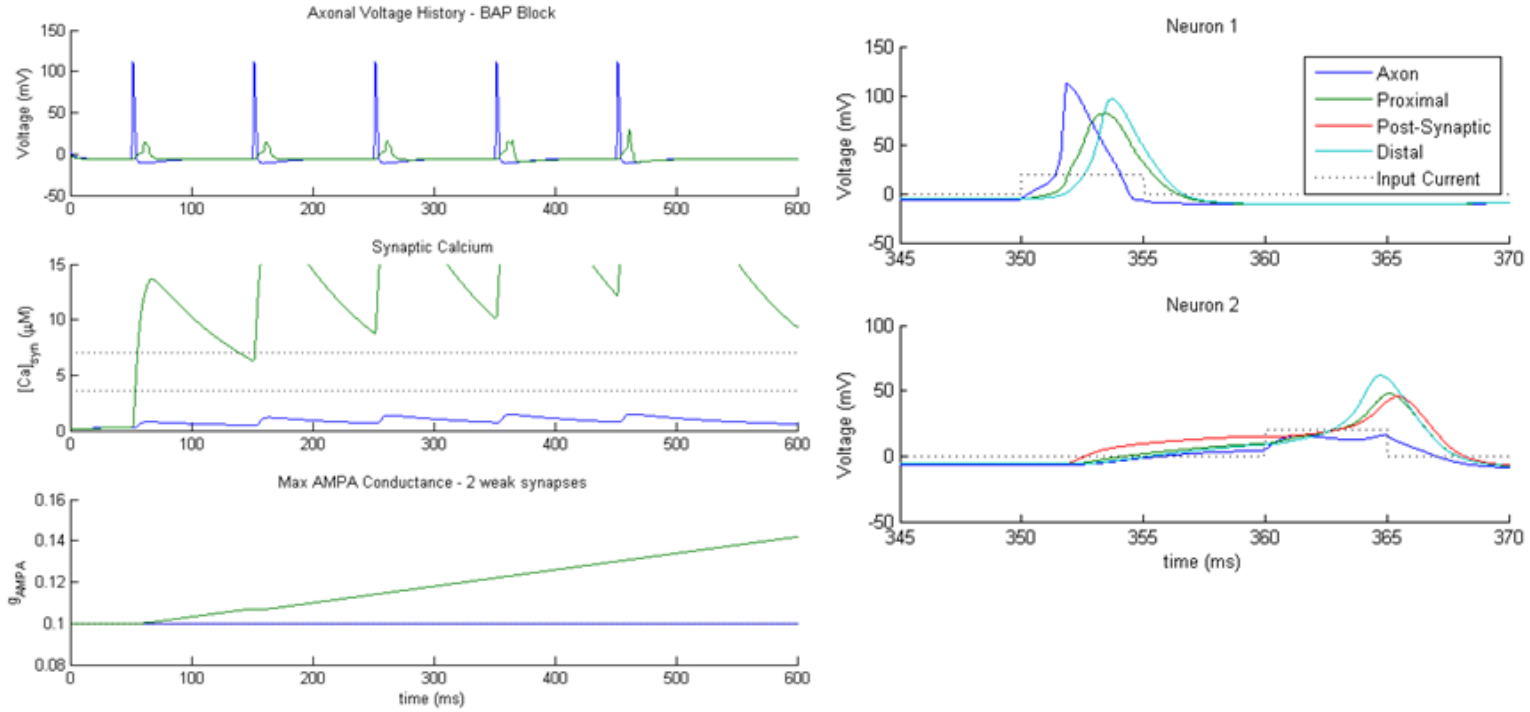

Figure 8 – Two weak synapses showing cooperativity can induce LTP in the absence of bAPs. (A) Voltage history in the somatic compartments of the two neurons. (B) Calcium history of the pre-before post synapse (green) and the post-before-pre synapse (blue). (C) Max AMPA conductance history of the two synapses. The pre-before-post synapse increases strongly even without the bAP. (D) Close-up of voltage traces for each compartment. The regenerative event of the red trace in Neuron 2 shows the dendritic spike. In this situation the small amount of current in the axonal compartment, along with the current coming in from the two synapses was needed to induce the dendritic spike.

blocking the bAP weak synapses are not able to generate dendritic spikes and that little to no potentiation occurs during these protocols. Due to the multiple compartments of the model we are able to account for much of the data generated by the experiments performed by Golding. In order to block the bAP Golding applied TTX locally to the soma. We accomplished similar effects of TTX by changing the maximum sodium conductance to 0 in the somatic compartment.

Three experiments were carried out on the model to demonstrate the necessity of dendritic spikes on the induction of LTP. After setting the sodium conductance in the axon to 0 (applying TTX), we used the same stimulation protocol used in Figure 3. Without the bAP the dendrites did not generate spikes (Figure 7d) and the protocol resulted in little to no plasticity – actually the pre-before-post synapses (which was potentiated without TTX) slightly depressed in this situation.

The other experiments were used to show how strong synapses could elicit LTP with bAPs blocked. For this experiment the initial AMPA conductance for the synapses were increased by 2.5 times the amount used in the protocol for Figure 3. Still with TTX applied, the network was put under the same protocol except now with the strong synapse. Under this situation the pre-before-post synapse strongly potentiated and also generated dendritic spikes (red curve in Figure 8d), while the post-before-pre synapse remained unchanged.

A second type of strong synapse was created by making two synapses from the pre-synaptic neuron to the post-synaptic compartment. Each of these synapses started off at the same initial strength used in the original protocol. With TTX applied the combination of two weak synapses was enough to generate a dendritic spike as well as LTP in the model. This gives further support to the use of cooperativity in inducing LTP as many weak synapses located close to each other – in the same dendritic compartment, can lead to enough current to generate LTP. Notably, the extra current injected into the soma during this experiment along with the current entering through the post-synaptic compartment was able to create dendritic spikes in the other dendritic compartments.

Discussion

The model presented in this paper serves as a very detailed implementation of the biophysics and dynamics underlying many features of a neuron and the connectivities between neurons. Using a simplified version of the dynamical process that transforms a calcium signal into a change in synaptic efficacy, the model is qualitatively able to emulate many of the experimentally observed behaviors of real neurons. Further detail of this model can be added to get a more even realistic representation of the dynamics of real neurons by including a more detailed description of the process between the calcium signal and the change in synaptic efficacies. The processes of calcium signaling have been described in much detail (10; 11) much of which has been previously modeled (12; 6). This model goes beyond these previous descriptions by incorporating multiple compartments to more fully describe the plasticity of neurons. This is an essential step to fully understand the functions of neuronal circuits as dendritic mechanisms governing plasticity come more into light. Several other studies suggest many different ways that plasticity is affected by dendritic properties (13; 14) which will require a multi-compartmental model in order to fully implement these properties. Another important property of

multi-compartmental models is the ability of the circuit to modulate the state of each compartment individually, which may lead to circuit regulated learning mechanisms.

The model described here made many assumptions about the channel densities found throughout the neuron. The somatic compartment used densities described by Hodgkin and Huxley (which may be inappropriate for modeling cortical neurons). The dendritic channel densities, however, were chosen somewhat arbitrarily. Experimentally derived channel densities would enable us to use a model such as this one to very accurately understand the dynamics of a neuron and create better theories of exactly the functions the neuron is trying to accomplish. It would be of further benefit to also know how much these densities varied across neuronal types as well as with neuronal types.

In Shouval et al's model of synaptic plasticity they had to make the assumption that the bAP had a slow after-depolarizing tail. This was essentially done because the action potential was too thin to generate enough calcium flux through the NMDA channel. Our model was able to remove the need for this assumption through the use of the different levels of channel densities in the dendritic compartments as compared to the soma. With lower densities of sodium and potassium channels in the dendrites, the dendritic spikes were typically slower, broader, and shorter. Slower and broader spikes gave more time for the magnesium block to be removed from the NMDA channel allowing more calcium influx. Also, a shorter action potential also lead to a stronger driving force on the calcium ions entering through the NMDA channel – higher depolarization pushes calcium out of the cell. Effects such as these shows further the need for descriptions of channel densities in the dendrites of neurons.

Another interesting observation of this model's behavior is the time course of dendritic spiking. Studies have shown that the time it takes for the transmission of action potentials can be as little as 0.1 ms and as long as 44 ms (15; 16; 17). Importantly, these timings are very consistent and highly reproducible (17; 18). It is likely that the brain uses this timing information for computation and many theories about brain function have started to use timing as an important part of information processing (19). In this model and observed experimentally (20) the onset of a dendritic spike can be a strong signal in inducing a somatic action potential – stronger than the EPSPs alone. However, the kinetics of producing a dendritic spike can vary in this model. Depending on the channel properties in the dendrites, stronger synapses or more cooperative signals may not only lead to a stronger depolarization of the post-synaptic cell, but may also lead to faster kinetics of a dendritic spike. Thus plasticity regulations may also be able to alter the temporal coding of incoming signals simply by changing the conductance.

The classical theoretical model of STDP was a good step towards understanding the underlying functional goal of neurons and networks. In light of more recent biological evidence, though, it is unlikely that timing alone determines the dynamics of synapses. Sjostrom et al show that there are at least three different strategies of inducing plasticity – timing, rate, and cooperativity, all of which can act together to regulate synaptic efficacies. This model captures much of the detail that underlies these processes and shows possible mechanisms that determine how to modify synapses. Simplification of this model is an important next step. Simplification is not beneficial simply because of computational efficiency, rather it is important, like STDP, for understanding the abstract functional goal neurons and networks are attempting to implement.

Contact efrady@ucsd.edu for supplemental information.

Bibliography

1. *Synaptic Modifications in Cultured Hippocampal Neurons: Dependence on Spike Timing, Synaptic Strength, and Postsynaptic Cell Type.* **Bi, Guo-qiang and Poo, Mu-ming.** 24, December 15, 1998, The Journal of Neuroscience, Vol. 18, pp. 10464-10472.

2. *Regulation of Synaptic Efficacy by Coincidence of Postsynaptic APs and EPSPs.* **Markram, Henry, et al.** 1997, Science, Vol. 275, pp. 213-215.

3. *Timing-Based LTP and LTD at Vertical Inputs to Layer II/III Pyramidal Cells in Rat Barrel Cortex.* **Feldman, Daniel E.** July 2000, Neuron, Vol. 27, pp. 45-56.

4. *A quantitative description of membrane current and its application to conduction and excitation in nerve.* **Hodgkin, A., Huxley, A.** 1952, Journal of Physiology, Vol. 117, pp. 500-544.

5. *Kinetic Models of Synaptic Transmission.* **Destexhe, A., Mainen, Z.F., Sejnowski, T.J.** 1998, Methods in Neuronal Modeling.

6. *Biophysical model of synaptic plasticity dynamics.* **Abarbanel, H.D.I., Gibb, L., Huerta, R., Rabinovich, M. I.** 2003, Biological Cynernetics, Vol. 89, pp. 214-226.

7. *A unified model of NMDA receptor-dependent bidirectional synaptic plasticity.* **Shouval, H. Z., Bear, M. F., Cooper, L. N.** 16, 2002, Proceedings of the National Acadamy of Sciences, Vol. 99, pp. 10831-10836.

8. *Rate, Timing, and Cooperativity Jointly Determine Cortical Synaptic Plasticity.* **Sjostrom, Per Jesper, Turrigiano, Gina G. and Nelson, Sacha B.** December 20, 2001, Neuron, Vol. 32, pp. 1149-1164.

9. *Dendritic spikes as a mechanism for cooperative long-term potentiation.* **Golding, Nace L., Staff, Nathan P. and Spruston, Nelson.** July 18, 2002, Nature, Vol. 418, pp. 326-331.

10. *Endogenous Ca2+ Buffer Concentrations and Ca2+ Microdomains in Hippocampal Neurons.* **Muller, A., Kukley, M., Stausberg, P., Beck, H., Muller, W., Dietrich, D.** 3, 2005, The Journal of Neuroscience, Vol. 25, pp. 558-565.

11. *Selective induction of LTP and LTD by postsynaptic [Ca2+] elevation.* **Yang, S.-N., Tang, Y.-G. and R.S., Zucker.** 1999, Journal of Neurophysiology, Vol. 81, pp. 781-787.

12. *A biophysical model of bidirectional synaptic plasticity: dependence on AMPA and NMDA receptor channels.* **Castellani, G. C., Quinlan, E. M., Cooper, L. N., Shouval, H. Z.** 2001, Proceedings of the National Acadamy of Sciences, Vol. 98, pp. 12772-12777.

13. *Spike-timing-dependent synaptic plasticity depends on dendritic location.* **Froemke, Robert C., Poo, Mu-ming and Dan, Yang.** March 10, 2005, Nature, Vol. 434, pp. 221-225.

14. *Dendritic mechanisms controlling spike-timing-dependent synaptic plasticity.* **Kampa, Bjorn M., Letzkus, Johannes J. and Stuart, Greg J.** 9, 2007, TRENDS in Neurosciences, Vol. 30, pp. 456-463.

15. *Efferent neurons and suspected interneurons in binocular visual cortex of the awake rabbit: Receptive fields and binocular properties.* **Swadlow, H. A.** 1988, Journal of Neurophysiology, Vol. 88, pp. 1162-1187.

16. *Monitoring the excitability of neocortical efferent neurons to direct activation by extracellular current pulses.* **Swadlow, H. A.** 1992, Journal of Neurophysiology, Vol. 68, pp. 605-619.

17. *Physiological properties of individual cerebral axons studied in vivo for as long as one year.* **Swadlow, H. A.** 1985, Journal of Neurophysiology., Vol. 54, pp. 1346-1362.

18. *Efferent neurons and suspected interneurons in motor cortex of the awake rabbit: Axonal properties, sensory receptive fields, and subthreshold synaptic inputs.* **Swadlow, H. A.** 1994, Journal of Neurophysiology, Vol. 71, pp. 437-453.

19. *Polychronization: Computation with Spikes.* **Izhikevich, Eugene M.** 2006, Neural Computation, Vol. 18, pp. 245-282.

20. *Dendritic Sodium Spikes Are Variable Triggers of Axonal Action Potentials in Hippocampal CA1 Pyramidal Neurons.* **Golding, Nace L. and Spruston, Nelson.** 1998, Neuron, Vol. 21, pp. 1189-1200.

21. **Hebb, Donald O.** *The Organization of Behavior.* New York : Wiley, 1949.

22. *Active propagation of somatic action potentials into neocortical pyramidal cell dendrites.* **Stuart, Greg and Sakmann, Bert.** January 6, 1994, Nature, Vol. 367, pp. 69-72.

23. *Dendritic coincidence detection of EPSPs and action potentials.* **Stuart, Greg and Hausser, Michael.** 1, January 2001, Nature Neuroscience, Vol. 4, pp. 63-71.